Low-temperature solution-processed wavelength-tunable perovskites for lasing

Xing, Guichuan; Mathews, Nripan; Lim, Swee Sien; Yantara, Natalia; Liu, Xinfeng; Sabba, Dharani; Grätzel, Michael; Mhaisalkar, Subodh; Sum, Tze Chien

2014

Xing, G., Mathews, N., Lim, S. S., Yantara, N., Liu, X., Sabba, D., et al. (2014). Low-Temperature Solution-Processed wavelength-Tunable perovskites for lasing. Nature Materials, in press.

https://hdl.handle.net/10356/79520

https://doi.org/10.1038/nmat3911

SUPPLEMENTARY INFORMATION

Low-Temperature Solution-Processed Wavelength Tunable Perovskites for Lasing

Guichuan Xing[1]†, Nripan Mathews[2,3,4]†*, Swee Sien Lim[1,3], Natalia Yantara[2,3], Xinfeng Liu[1], Dharani Sabba [2,3], Michael Grätzel[3,5], Subodh Mhaisalkar[2,3],Tze Chien Sum[1]*

[1]Division of Physics and Applied Physics, School of Physical and Mathematical Sciences, Nanyang Technological University, 21 Nanyang Link, Singapore 637371.

[2]School of Materials Science and Engineering, Nanyang Technological University, Nanyang Avenue, Singapore 639798.

[3]Energy Research Institute @NTU (ERI@N), Research Techno Plaza, X-Frontier Block, Level 5, 50 Nanyang Drive, Singapore 637553.

[4]Singapore-Berkeley Research Initiative for Sustainable Energy, 1 Create Way, Singapore 138602, Singapore.

[5]Laboratory of Photonics and Interfaces, Department of Chemistry and Chemical Engineering, Swiss Federal Institute of Technology, Station 6, CH-1015 Lausanne, Switzerland.

*Correspondence to: Tzechien@ntu.edu.sg; Nripan@ntu.edu.sg

†These authors contributed equally.

SUPPLEMENTARY INFORMATION

1. Optical Properties

After spincoating, a clear optically flat film of $CH_3NH_3PbI_3$ was obtained with thickness of ~65 nm. The $CH_3NH_3PbI_3$ film has strong absorbance (~ 10^4 cm^{-1}) from UV to near infrared (800 nm) with two distinct peaks located at 480 nm and 760 nm (Supplementary Fig. 1**a**), which are consistent with previous publications[8-11]. The broad strong absorbance is a good indication of its excellent light harvesting capabilities. The second absorption peak (760 nm) is attributed to the direct gap transition from the first valence band maximum to the conduction minimum. The first absorption peak (480 nm) is attributed to the transition from lower valence band to the conduction band minimum[8]. The strong band edge PL peaks at 770 nm (Supplementary Fig. 1**a**).

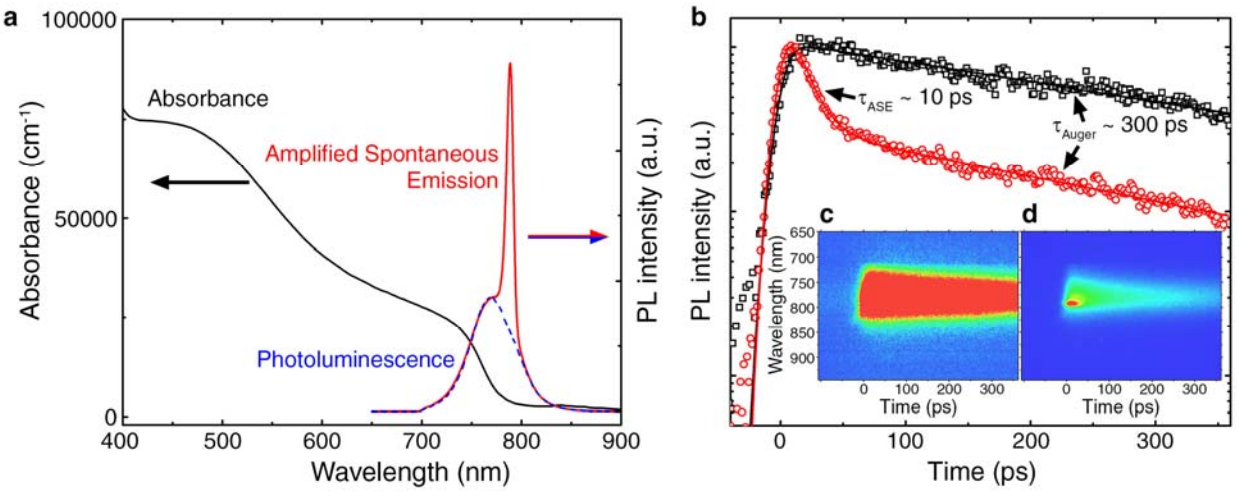

Supplementary Figure 1 | Steady state and transient PL. a, A comparison of the ASE profile in relation to the absorption and SE profile for $CH_3NH_3PbI_3$. The ASE develops at the wavelength where the optical gain and absorption are balanced – the ASE peak is red-shifted with respect to the PL peak. **b**, Typical TRPL decay transients following photo-excitation with pump fluence below (~10 μJ cm^{-2}, black) and above (~13 μJ cm^{-2}, red) the ASE threshold (*i.e.*, 12 ± 2 μJ cm^{-2}). Inset shows the streak camera images of spectrum vs time (collected over a time

window of 460 ps) for the (**c**) below and (**d**) above ASE threshold fluence. Do note that the lifetime data presented in Supplementary Fig. 1**b** is collected over a time window of 18 ns to allow consistent comparison with the longer-lived SE dynamics.

Room temperature photoluminescence quantum yield (PLQY)[30] of the perovskite thin films were measured using an integrating sphere. The samples were excited with 600 nm pulses generated from the Coherent OPerA-Solo. The emission was corrected for CCD and grating responsivity.

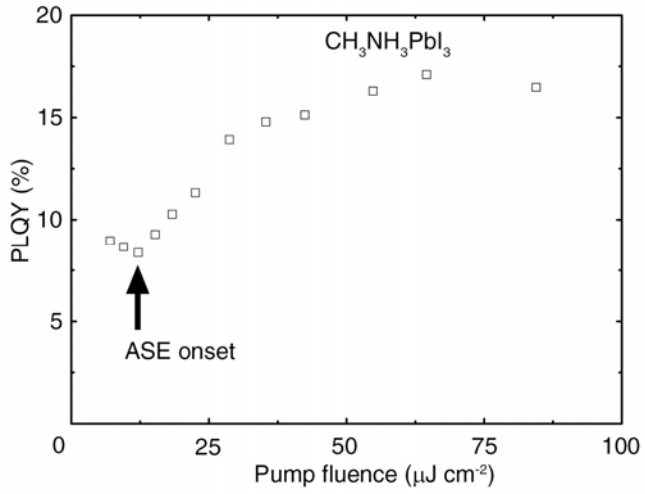

Supplementary Figure 2 | Photoluminescence Quantum Yield (PLQY) dependence on pump fluence. Room temperature PLQY measurements of $CH_3NH_3PbI_3$ films at various pump fluence.

The room temperature gain of the $CH_3NH_3PbI_3$ sample was assessed using Variable Stripe Length (VSL) measurements (Supplementary Fig.3). The data is fitted using two methods. The method developed by Shaklee and Leheny[18], is a straightforward way to determine the gain

spectrum of a material over the small signal regime (utilized for inorganic and organic semiconductors in slab geometry). The equation is:

$$I_0(z) = \frac{I_s A}{g}\left[\exp(gz) - 1\right] \quad (1)$$

where $I_0(z)$, g, and z are the detected light intensity, gain coefficient and excitation stripe length, respectively; I_s is the spontaneous emission rate per unit volume and A is the cross-sectional area of the excited volume.

Another method developed by Chan *et al.*[7] for analysis over the entire signal regime (including saturation) and is more commonly used in solution processed colloidal quantum dot films. The equation is:

$$I = \exp\left[gl_\alpha \left(1 - \exp\left\{ \frac{-(z - z_0)}{l_\alpha} \right\} \right) \right] \quad (2)$$

Where I, g, and z are the ASE intensity, gain coefficient and excitation stripe length, respectively; while z_0 accommodates for possible pump beam inhomogenity and delayed ASE onset. l_α is a parameter that accounts for the saturation in ASE intensity which is defined as the gain lifetime multiplied by the speed of light within the gain medium.

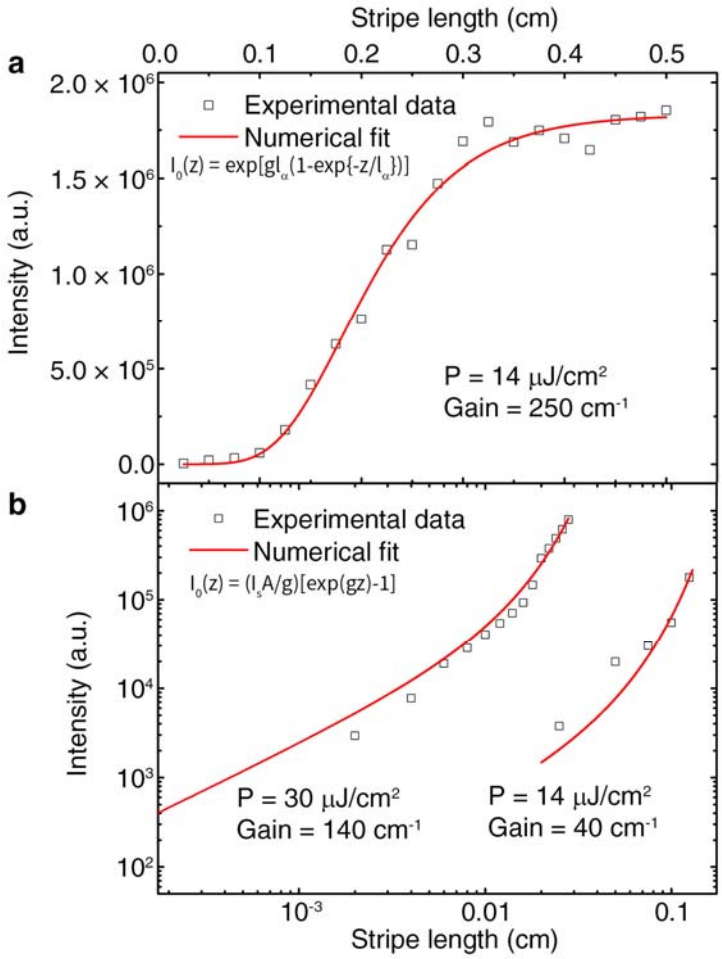

Supplementary Figure 3 | Determination of the Gain. a, **b**, Room temperature variable stripe length (VSL) measurements of the $CH_3NH_3PbI_3$ films and fitted using the respective methods used (**a**) for solution processed colloidal quantum dots thin films and (**b**) for organic thin films.

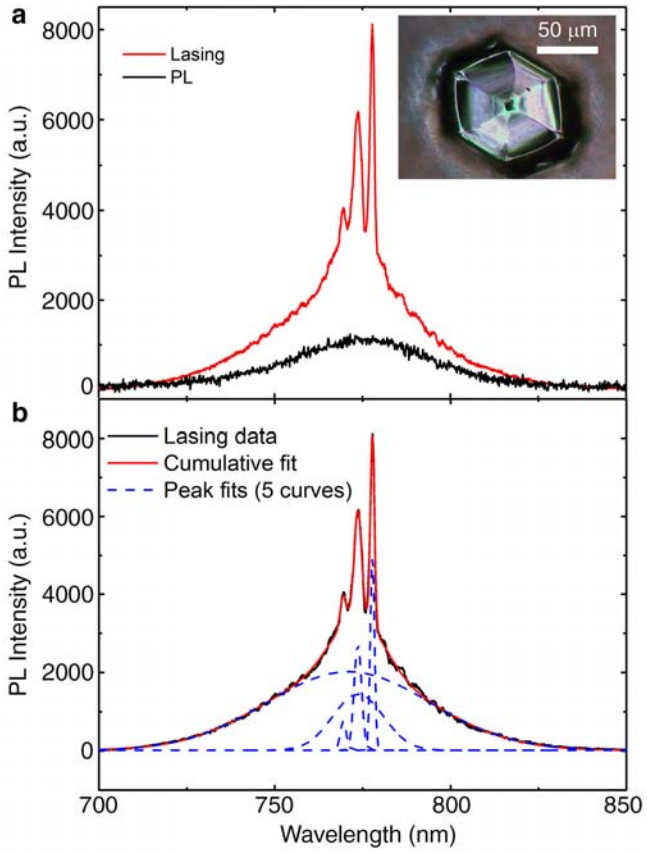

Supplementary Figure 4 | Lasing from $CH_3NH_3PbI_3$ single crystals. a, Room temperature lasing from $CH_3NH_3PbI_3$ single crystals from dropcasted films. Inset is the optical micrograph of the crystal. **b**, Lasing spectra fitted to 5 peaks. The most prominent mode shows a full width half maximum of 1.2 nm.

2. Trap States Density Determination.

Under low fluence fs laser pulse excitation (where Auger recombination is negligible) and the assumption that trap states recombination is much slower than band edge radiative recombination, the dynamics of photo-generated charge carrier density (n_C) can be described with the following set of differential equations:

$$\frac{dn_c(t)}{dt} = -\sum_i a_i n_c(t) n_{TP}^i(t) - \frac{n_c(t)}{\tau_0} \quad (3)$$

$$\frac{dn_{TP}^i(t)}{dt} = -a_i n_c(t) n_{TP}^i(t) \quad (4)$$

where $n_{TP}^i(t)$ is the trap states density and a_i is the product of the trapping cross section and the carrier velocity. Therefore the first term in equation (3) represents various trap-mediated non-radiative pathways, while the second term denotes the radiative recombination inside the film. Thus the relationship between the integrated bandedge PL intensity ($I_{PL} = k\int_0^\infty n_c(t)/\tau_0 dt$, where *k* is a constant), the initial photogenerated charge carrier density $n_C(0)$ can be obtained as:

$$n_c(0) = \sum_i n_{TP}^i(0)(1 - e^{-a_i \tau_0 I_{PL}/k}) + I_{PL}/k \quad (5)$$

Fitting the experimental result with equation (5) yields two types of traps in these $CH_3NH_3PbI_3$ thin films, with the bulk (surface/interfacial) traps exhibiting fast (slow) trapping times[8,21,22]. The bulk trap density is $n_{TP}^F \sim 5\times10^{16}$ cm^{-3} while the surface/interfacial trap density is $n_{TP}^S \sim 1.6\times10^{17}$ cm^{-3}. This correlates well with a simple estimation of the total trap density (bulk and surface) obtained by the intersection of the linearly extrapolated PL intensity (in blue) with that of the pump fluence axis from Fig. 1**c** in the main text (i.e., $n_{TP}^0 \sim 2\times10^{17}$ cm^{-3}). This intersection represents the pump fluence needed to fill all the traps (*i.e.*, the threshold trap pump fluence P_{th}^{Trap}).

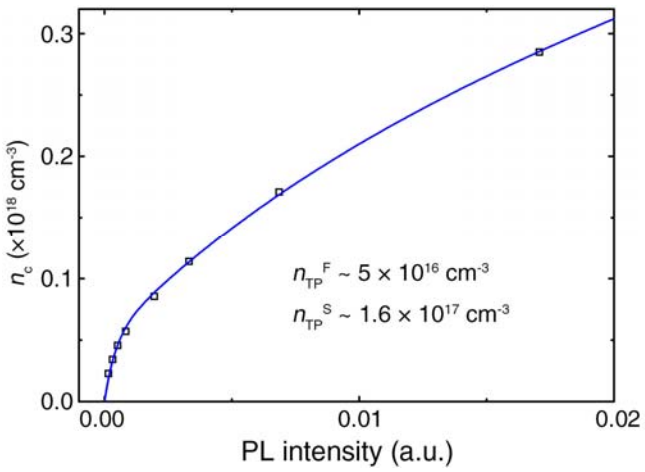

Supplementary Figure 5 | Determination of the trap state densities. PL intensity as a function of photon-generated exciton density within the low pump fluence range. The experimental data can be well-fitted (R^2 = 0.99) with equation (5) for two types of trapping states.

3. FDTD Simulations

Finite difference time domain (FDTD) simulations (Lumerical^{TM} FDTD software) were performed to evaluate the optical confinement effects of the PCBM layer. The structure comprises of Quartz (100nm)/$CH_3NH_3PbI_3$ (65nm)/PCBM (45nm - optional)/vacuum (390nm). The refractive index of $CH_3NH_3PbI_3$ was measured using an ellipsometer - $n_{CH_3NH_3PbI_3} = 2.3$ and $k_{CH_3NH_3PbI_3} = 0.15$ at 790 nm (Supplementary Fig. 6**a**) while that of PCBM was extracted from the literature[31]. A light source is introduced in-plane to the $CH_3NH_3PbI_3$ film and perfectly matched layers (PML) boundary conditions are used to absorb the incident light at the top and bottom edges with minimal reflections. Supplementary Fig. 6**c** shows the light intensity distributions in the *y*-*z* plane for the films with and without the PCBM layer for light polarized parallel to thin film surface. With the PCBM layer as a cladding, this polarized light component propagates a

longer distance in the $CH_3NH_3PbI_3$ film, demonstrating better light confinement. The out-of-plane polarized component exhibits extremely poor confinement within the $CH_3NH_3PbI_3$ film and leaks out rapidly.

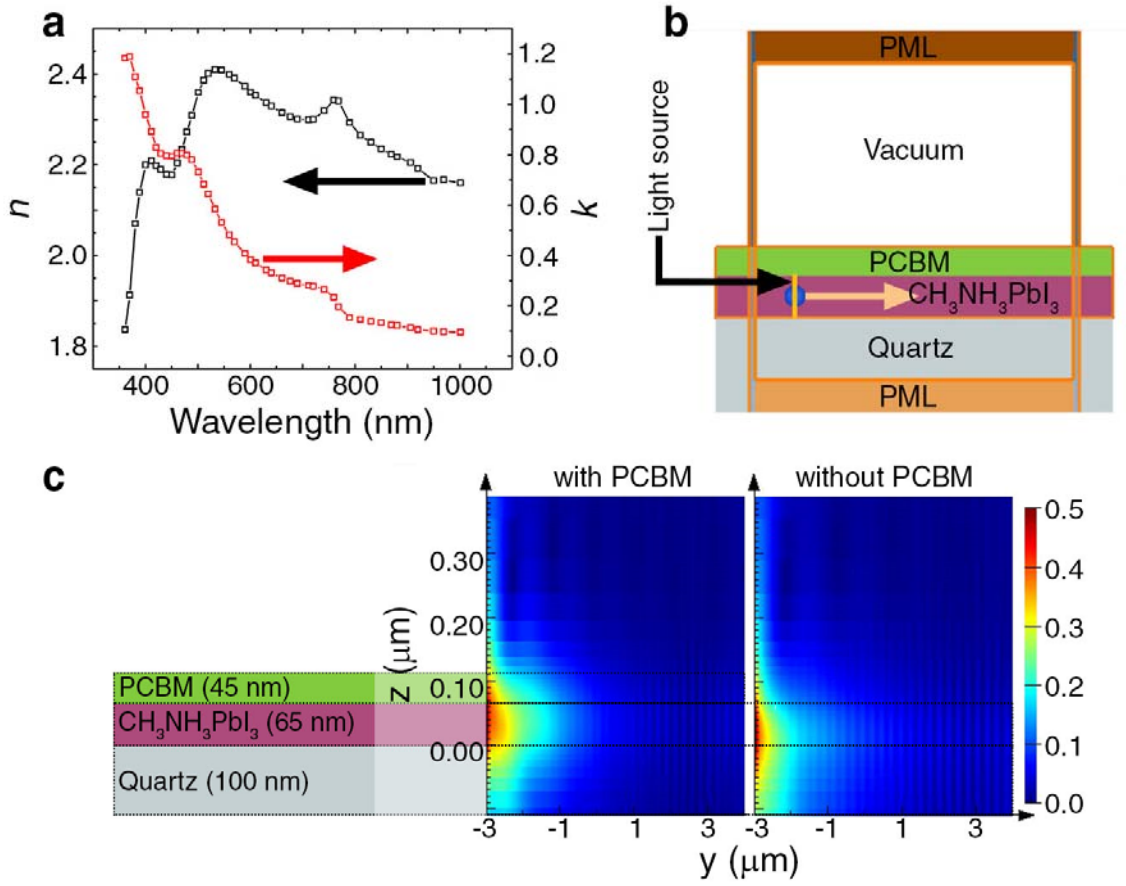

Supplementary Figure 6 | Better light confinement with the PCBM layer. a,The real part (n) and imaginary part or extinction coefficient (k) of the complex refractive index. **b,** A schematic showing the film structure, the simulation conditions (*i.e.*, placement of the light source (yellow line in the $CH_3NH_3PbI_3$ layer) and the perfectly matched layers (PML) boundary conditions). **c,** Light intensity distributions in the *y-z* plane for the films with and without the PCBM layer for light polarized parallel to the film surface.

4. Temperature dependent effects on the PL and coherent light emission.

Temperature dependent studies were also performed to further characterize the solution-processed $CH_3NH_3PbI_3$ gain medium. Figure 3**b** in the main text shows the temperature dependent PL of the film from 6 K to 300 K. $CH_3NH_3PbI_3$ undergoes a phase transition from tetragonal to orthorhombic around 160 K[26] which clearly manifests as a modulation of the PL spectra (i.e., from one emission peak in the tetragonal phase to three emission peaks in the orthorhombic phase). In both phases, the emission peak energies decrease only slightly with decreasing temperatures. The highest energy PL peak (746 nm) in orthorhombic phase is attributed to free exciton emission, while the other two peaks are attributed to bound exciton emissions. Due to the limited bound states in the film, the emission intensity of these two peaks exhibit clear saturation behaviors at higher pump fluence (Supplementary Fig. 7**a** and 7**b**). However, the free exciton emission intensity increases continually with increasing pump fluence, finally achieving ASE above a threshold fluence of 10 ± 2 μJ/cm^2. This ASE threshold at 6 K is comparable to that at 300 K (i.e., 12 ± 2 μJ cm^{-2}). Comparatively, traditional inorganic semiconductor gain media are highly susceptible to temperature induced effects: strong phonon assisted charge carrier trapping; temperature dependent exciton dissociation and photo-generated charge carrier diffusion and dilution. Hence, the threshold pump fluence for generating coherent light emission from these inorganic semiconductor materials are strongly temperature dependent. However, for $CH_3NH_3PbI_3$, the ASE threshold is almost temperature-insensitive, which are similar to organic chromophores and quantum dots[1-7]. The temperature-insensitivity of $CH_3NH_3PbI_3$ ASE threshold stems from its extremely low trap states density and almost temperature invariant charge carrier diffusion (Supplementary Fig. 7**c**).

SUPPLEMENTARY INFORMATION

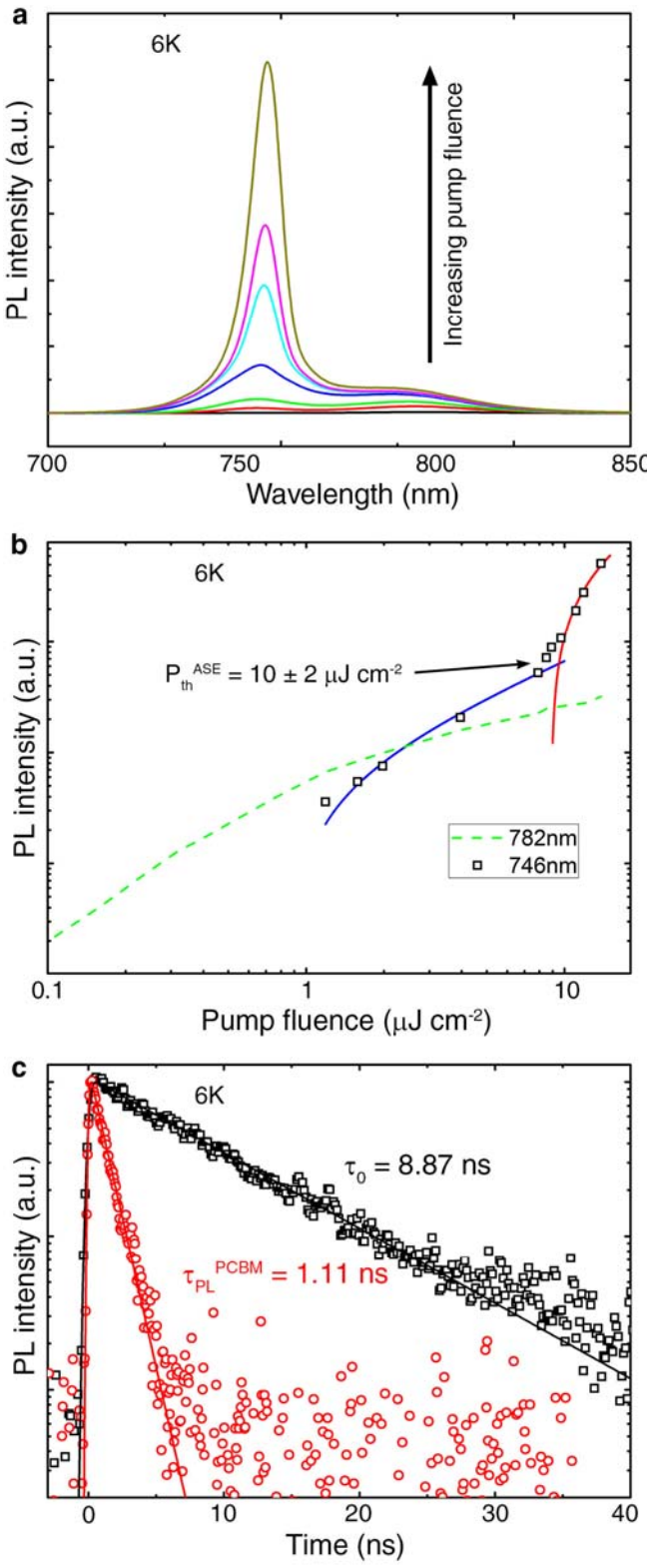

Supplementary Figure 7 | Temperature dependent effects on the SE and ASE. a, **b**,The pump fluence dependent PL spectra (**a**) and PL intensity (**b**) at 6 K. **c**, TRPL decay transients for quartz/$CH_3NH_3PbI_3$(65 nm) (black) and quartz/$CH_3NH_3PbI_3$(65 nm)/PCBM(45 nm) (red) films in vacuum following excitation at 600 nm (1 KHz, 150 fs, ~1 μJ cm^{-2}). The solid lines in (**c**) are the single-exponential fits of the PL decay transients.

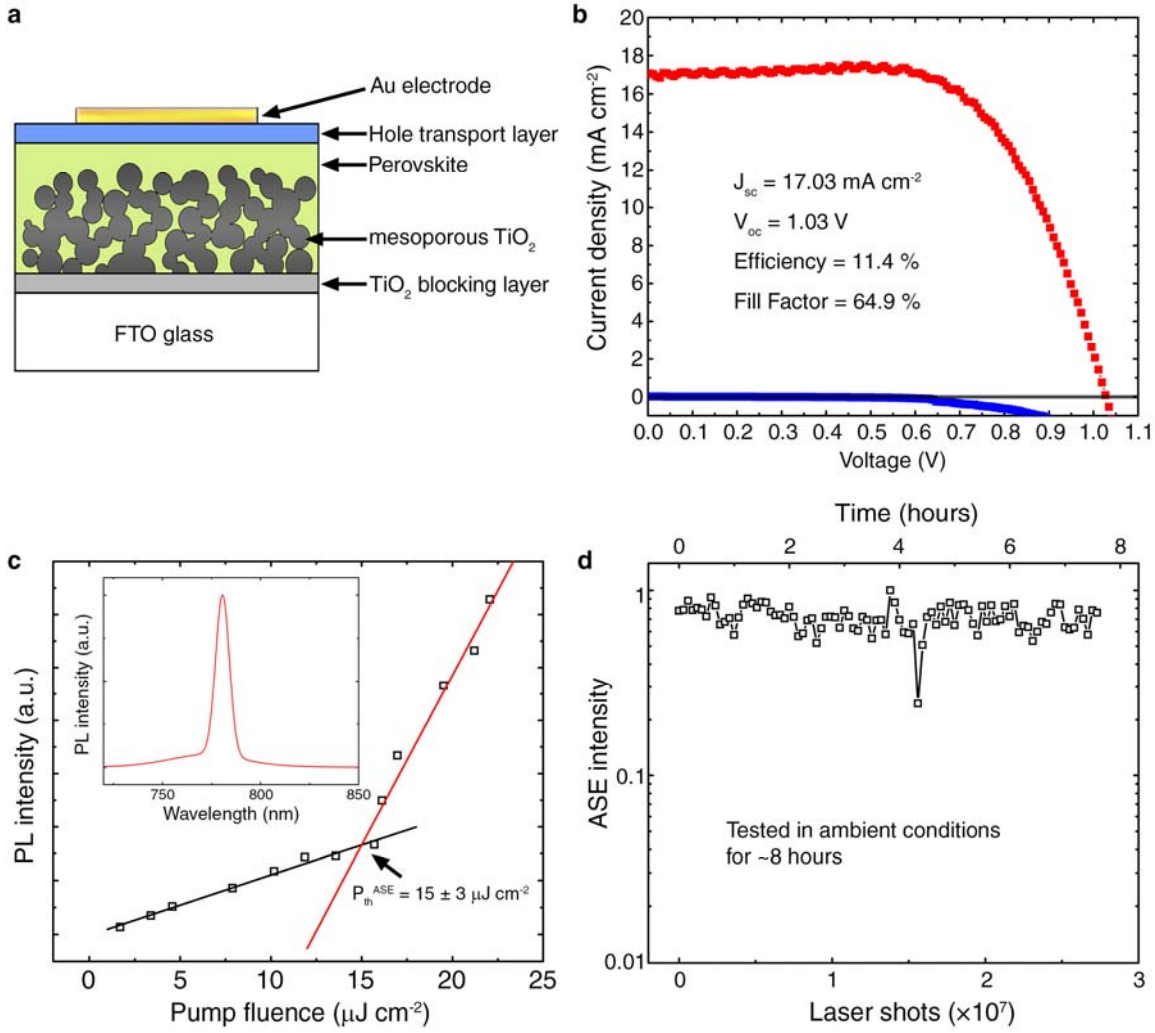

Supplementary Figure 8 | ASE measured in solar cell configuration. a, Schematic of the $CH_3NH_3PbI_3$ solar cell consisting of FTO/TiO_2 compact layer/TiO_2 mesoporous layer/$CH_3NH_3PbI_3$/Spiro-OMetad/Au. **b**, J-V characteristics of the solar cell under AM 1.5 (100

mW/cm^2) illumination. **c,** PL intensity as a function of pump fluence showing ASE threshold of the solar cell configuration. Inset shows the representative ASE spectrum. **d**, ASE photostability measured under ambient conditions of the device (Excited with 600 nm, 1 KHz, 50 fs laser pulses, ~20 μJ cm^{-2}).

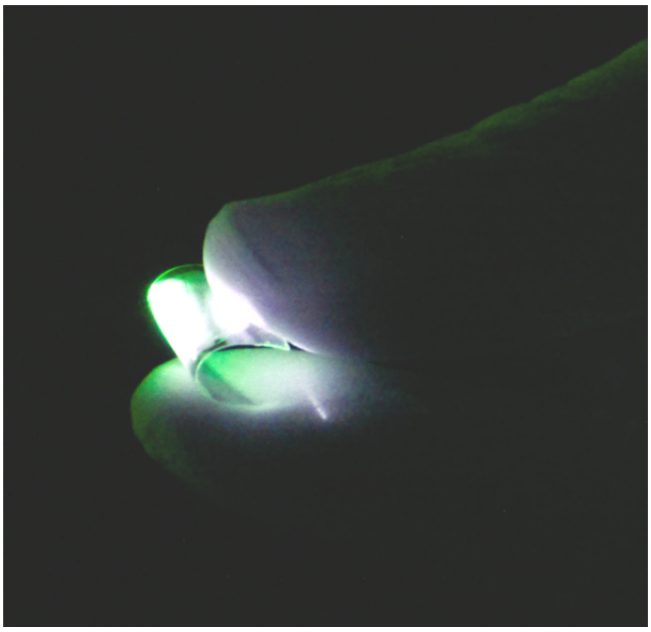

Supplementary Figure 9 | ASE from flexible substrates. A demonstration of green ASE from $CH_3NH_3PbBr_3$ deposited on PET substrates pumped using two-photon absorption at 800 nm.

References

30. Würth, C., Grabolle, M., Pauli, J.,Spieles, M.,&Resch-Genger, U. Relative and absolute determination of fluorescence quantum yields of transparent samples. *Nat.Protoc.***8**, 1535-1550 (2013).

31. Hoppe, H.,Sariciftci, N. S.,&Meissner, D. Optical constants of conjugated polymer/fullerene based bulk-heterojunction organic solar cells. *Mol. Cryst. Liq. Cryst.***385,** 233-239 (2002).